STRUCTURAL TESTING OF C-5A AFT FUSELAGE SKIN PANELS

Melinda Laubach*, Betty Woodrow*, Tim Hickey*, Jon Karnes*, Larry Braden*, Anthony Alford*, Ed Ingram, James Greer*****
***Wichita State University – National Institute for Aviation Research (NIAR), Wichita KS**
****Lockheed Martin, (Marietta GA)**
*****Center for Aircraft Structural Life Extension (CAStLE), U.S. Air Force Academy CO**

Abstract

This paper provides a description of how the structural integrity testing of C-5A aft fuselage crown skin panels was conducted.

This research program was sponsored by the Nondestructive Evaluation (NDE) Branch of the Air Force Research Laboratory (AFRL) at Wright-Patterson Air Force Base and was administered through Universal Technology Corporation (UTC) under Contract F33615-03-D-5204 for an effort entitled "Inspection and Analysis Methods in Aging Military Aircraft." Lockheed Martin engineering support was funded by the 730th Aircraft Sustainment Group at Robins AFB through the C-5 Aircraft Structural Integrity Program (ASIP), Contract FA8525-05-D-0002.

Wichita State University National Institute for Aviation Research (NIAR) conducted full scale structural integrity testing and analysis on four C-5A aft fuselage crown skin panels in the Aircraft Structural Testing and Evaluation Center (ASTEC) facility located on the Hawker Beechcraft Corporation (HBC) campus in Wichita, KS.

The structural tests incorporated selected technologies in nondestructive inspection (NDI) techniques and structural health monitoring (SHM) systems to assess capabilities in both detecting and quantifying damage extent in metallic semi-monocoque aircraft structures.

1 Background

The C-5 Galaxy is a heavy-cargo transport aircraft, designed to carry enormous payloads great distances. As the largest airlifter in the U.S. Air Force, it can carry twice as much cargo as any other airlifter. In addition to the heavy and out-sized cargo capability, the aircraft features front and aft-loading as well as kneeling capabilities that dramatically reduce cargo transfer time. These and other features make this aircraft a vital national asset for both military and humanitarian relief missions.

The first production version, the C-5A, was designed in the late 1960s and first entered service with the U.S. Air Force in 1969. The "A" model design utilized extremely high strength aluminum alloys in order to save airframe weight and maximize payloads. The fuselage construction utilized 7079-T6 aluminum skin (clad one side), stiffened by 7075-T6 extruded stringers spaced at approximately seven inch intervals. The 7079-T6 sheet material has an ultimate tensile strength of 80 ksi, and similarly high compression and shear strengths. Utilizing this high strength and selecting higher operating stress levels to save weight, the original designers incorporated other features and details into the structural concept to meet the fatigue and damage tolerance requirements. TaperLok© fasteners were used in the skin splices to improve fatigue endurance and titanium fail safe straps were incorporated to provide crack-arrest capability.

By the time the C-5B production began in the 1980s, the airframe design philosophy had somewhat changed. The C-5B design substituted more corrosion-resistant alloys for the 7079-T6 material and increased the skin gages; thereby reducing the stress levels and

creating a more durable, damage-resistant structure.

From a fatigue standpoint, the C-5A design has proven successful. Based on results from the full scale fatigue test, as well as recent analytical studies at Lockheed Martin, the airframe is expected to remain free of widespread fatigue damage until well past its current planned retirement date. However, as has happened in a number of other aircraft designs, a type of structural degradation has occurred in 7079-T6 skin that could not have been foreseen 45 years ago. Cracks have been found during structural inspections of the aft upper fuselage (aft crown) region. This region is shown in Figure 1.

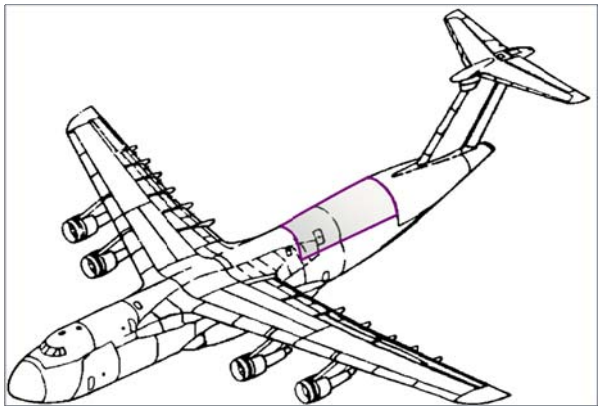

Fig. 1. C-5A fuselage aft crown region

Lockheed Martin and the U.S. Air Force undertook fractographic and metallurgical analyses of the damaged skin and concluded that the cracks were not due to fatigue cycles, but were a type of stress corrosion cracking (SCC). This conclusion is further supported by the observation that, in many cases, the cracks have occurred in locations and orientations where the operational applied stress levels are known to be very low. The cracks in the low-stress regions may be thought of as nuisance cracks that can be managed by a "find and fix" approach through the normal maintenance programs. But, the random nature of the orientations and locations of these cracks also means that some will occur in high-stress regions and in the most critical orientation (perpendicular to the maximum principal applied tension stress). Adding to the analytical complexity is the fact that no reliable method currently exists to predict SCC growth rates in a circumstance such as this, where the crack-driving stress is likely a fabrication-induced self-stress that varies from location to location within the skin panel. Also, the initiation sites are likely to be very small spots where the protective finish has been damaged or has deteriorated. All attempts at correlating the crack occurrences with time since manufacture, home base environment (coastal, inland, etc.), mission types, etc., have failed to produce any clues that would point toward a predictive parameter.

The approach to certification of the C-5A structure utilized the "slow crack growth" approach, rather than "fail safe." This approach, which has been used most often since the advent of fracture mechanics-based structural life-prediction techniques, generally leads to a lighter structural weight (mass fraction) than the fail safe approach. In the slow crack growth approach, an upper bound flaw size (rogue flaw) is hypothesized to exist at any structural detail at the time of manufacture. Crack growth analysis, using the operational cyclic stresses, geometric correction factors for the detail, and material growth rate properties provide a reasonable estimate of the crack length as a function of flight hours. When fatigue is the dominant factor in crack growth, the rate of growth will most often result in a reasonably "graceful" growth curve and the ability to devise a rational, economic inspection program that can detect cracks before they become critical, as shown in Figure 2.

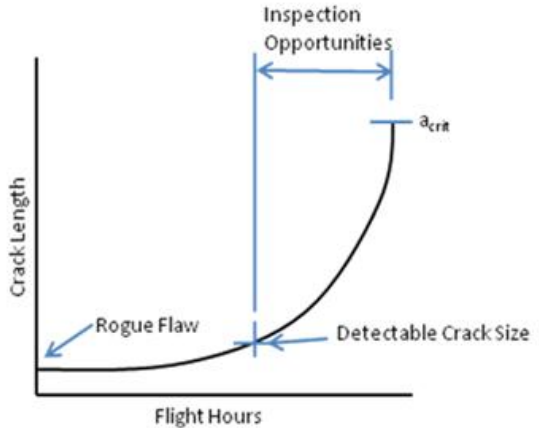

Fig. 2. Crack growth curves and inspection opportunities, fatigue crack growth

In the case of the aft crown, however, fleet evidence shows that some of the stress corrosion cracks in the aft crown make an abrupt transition to fast crack growth as shown in Figure 3.

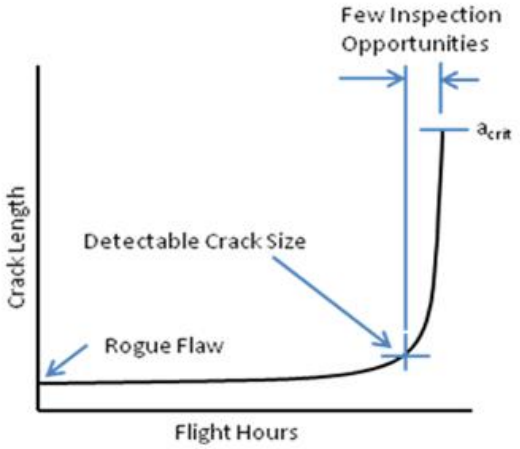

Fig. 3. Crack growth curves and inspection opportunities, stress corrosion crack growth

Rapid growth such as this requires frequent inspections to catch cracks in the window of opportunity between detectable and critical crack lengths. The current crack growth analysis terminates at the first instant the crack tip stress intensity (at design limit load) exceeds the material toughness, K_c. That is, despite the fact that the aft crown is a stringer-stiffened construction, the legacy residual strength analysis has not credited the stringers with crack arrest capability. If it could be proven that the stringers do in fact maintain crack stability for longer lengths; then the inspectability of the structure would be greatly improved.

A significant factor in the assessment of the crack arrest capability of the stringers is the toughness of the skin material. The high strength 7079-T6 sheet is brittle by comparison to lower strength aluminum alloys. The critical crack length, a_{cr}, is determined from the material toughness and the geometry of the local detail as follows:

$$a_{cr} = \frac{1}{\pi}\left(\frac{K_c}{\sigma_L \beta}\right)^2$$

Where σ_L is the design limit stress and β is the geometric correction factor that accounts for features such as holes and crack-arresting stiffeners.

If no consideration (or credit) is given to the arrest capabilities of the stringers, then the calculation of a_{cr} for the aft crown by the method above leads to values significantly less than the stringer spacing. A large critical crack length is obviously desirable under any circumstances, as it lengthens the crack growth time from detectable to critical, and greatly improves the detectability. In the particular circumstance of the aft crown, with the fast SCC growth rate, there is an especially great desire to increase the size of a_{cr}, if sufficient test evidence were available to do so.

Stringers that span a crack as shown in the sketch of Figure 4, can, if sufficiently stiff, reduce the applied stress intensity below the toughness value and thereby make the critical crack length exceed the stringer spacing.

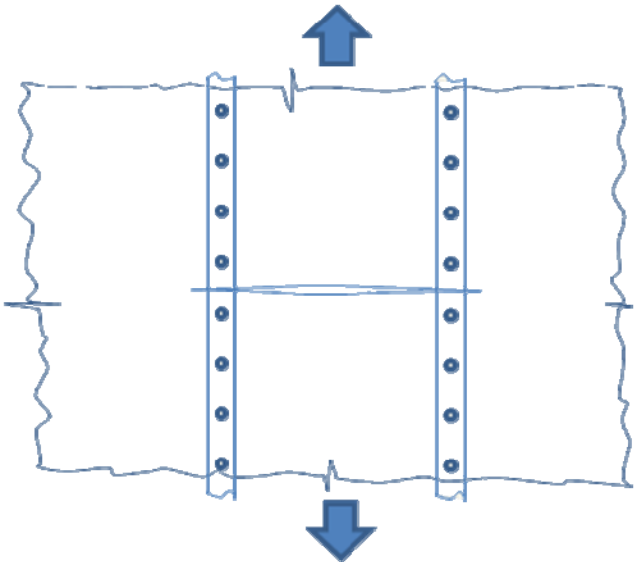

Fig. 4. "Sturdy" crack-spanning stiffeners increase the critical crack length

Until recently, the estimates of the critical crack lengths in the various skin/stringer bays of the aft crown were based on finite element analyses (FEA). The FEA results showed the stringers reduced the crack tip stress intensity but not enough to maintain crack stability. There are several aspects to a finite element-based calculation of critical crack length that require engineering judgment. How the fasteners are simulated (springs, bars, etc.), how to account for fastener load eccentricity, effect of stringer centroid offset from the skin plane, etc., all require choices that, without test data,

are often conservative. Figure 5 presents the C-5 fuselage crack stability problem in terms of applied stress intensity vs. crack length.

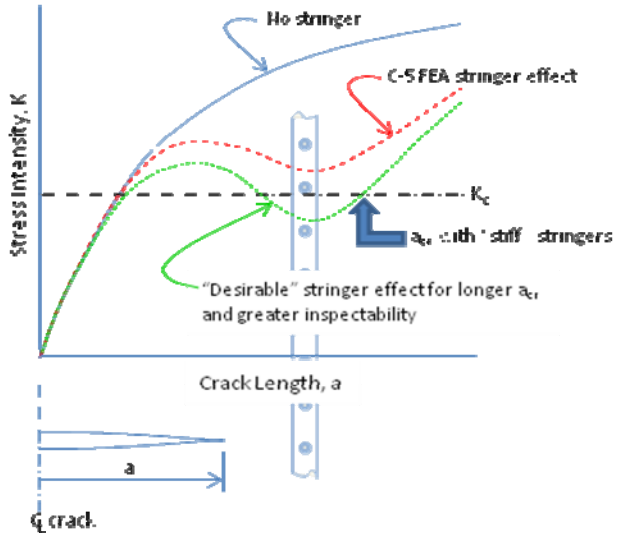

Fig. 5. Crack stability curve with stiffener effects

As shown in Figure 5, the FEA indicates the stringer does not provide enough stiffness (crack closing effect) to arrest a crack. Test evidence is needed that can prove the previous analytical estimates are conservative and critical crack length is significantly longer.

Once the U.S. Air Force and Lockheed Martin concluded that realistic residual strength tests were needed, it was proposed that NIAR conduct these tests as well as perform NDI studies and finite element modeling work to take maximum knowledge benefit from the test results.

2 General Introduction

The testing utilized four (three large and one small) selected C-5A aft fuselage crown skin panels for structural integrity testing. The structural integrity testing determined the residual strength capabilities of the test articles for multiple damage scenarios and assessed advanced NDI techniques. The tests also evaluated the feasibility and capability of SHM systems for detecting and identifying the extent of damage in major airframe components.

In order to convey direction and avoid confusion with respect to loads, bending, and other vector based subjects, an XYZ reference axis system was developed for this test program. Figure 6 presents the reference axis system that was used during this test program.

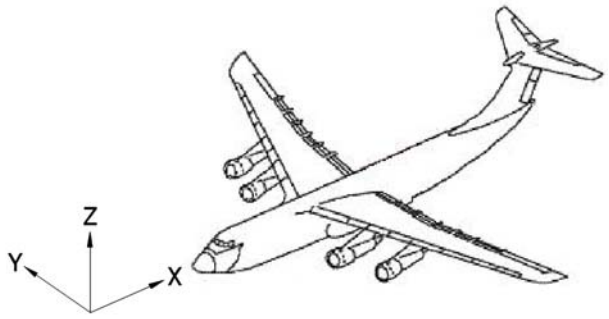

Fig. 6. Test program reference axis system

3 Test Panel Selection Process

The test panel selection process consisted of a survey and inspection of eleven retired C-5A aircraft in storage at the Aerospace Maintenance and Regeneration Group (AMARG). NIAR personnel documented all damage identified during the magneto optic imaging (MOI) inspections.

After the technical advisory group (TAG) reviewed the inspection results and any follow-on inspections; four panels were selected for removal and shipment to the NIAR-ASTEC facility based on the observed damage. The TAG was comprised of members from Lockheed Martin, Center for Aircraft Structural Life Extension (CAStLE), and NIAR. The following selection criteria were used to determine which panels were removed and shipped to the NIAR-ASTEC facility:

1. Cracks had to be located a distance of two undamaged stringer bays and one undamaged frame bay from the boundary of the inspection area.
2. Panels with widespread surface corrosion were not considered for selection.
3. Panels with more than five cracks oriented perpendicular or off-axis to the induced loading direction were not considered for selection; however, longitudinal cracks were assumed not to affect testing.
4. Panels with circumferential cracks were desired and selected; however, test articles with off-axis cracks could also be selected.

Off-axis cracks were judged to be less critical and less important to the structural integrity of the aft crown region than circumferential cracks since applied test loads were oriented axially.

5. Large "pristine" areas were desirable to induce damage scenarios of interest without interaction with surrounding pre-existing damage.

Following the selection, cut lines were drawn on four of the aircraft by NIAR personnel to outline the panels that would be removed for testing.

The cut lines included each test panel section plus additional panel area to allow for a precision trim at the NIAR-ASTEC facility and to provide specimens for material property analysis which was conducted by CAStLE personnel.

AMARG personnel removed these sections from the aircraft and shipped the four aft fuselage skin panels to the NIAR-ASTEC facility for assessment and full scale structural testing.

3.1 Test Panel Configurations

After the four panels were received at the NIAR-ASTEC facility, the panels were subjected to a thorough NDI program conducted by NIAR personnel using MOI and eddy current surface scan (ECSS) inspection methods to document the "as-delivered" configuration of each panel. The configuration of each panel was documented using dimensions, diagrams, and photographs on inspection forms for a pretest baseline. Figure 7 shows a typical configuration of the larger overall panels as cut from the aircraft, with the larger test articles and smaller fracture toughness coupon boundaries marked. The smaller panel was similar in configuration except shorter.

The test articles were identified with NIAR static test (ST) serial numbers. The larger test articles were designated ST-013, ST-014, and ST-015. The smaller test article was identified as ST-016.

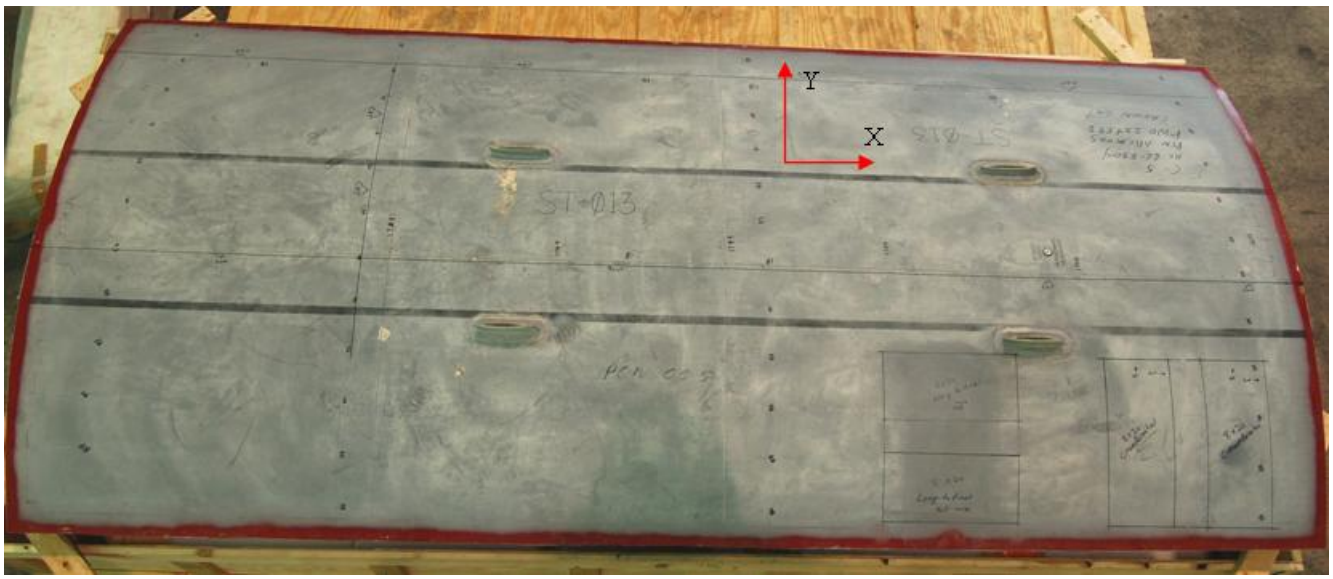

Fig. 7. Overall aircraft panel configuration

3.2 Damage Scenarios

A set of damage scenarios for testing was developed during meetings involving TAG team members.

The following damage scenarios were utilized for testing:

- Damage Scenario #1, ST-013 test article: A crack emanating from both sides of an open hole in a pristine bay bounded by stringers on the sides and a frame and tear strap forward and aft to assess the residual strength of the skin with minimal influence from surrounding support structure.
- Damage Scenario #2, ST-014 test article: A crack originating from both sides of a fastener hole common to the skin and a stringer propagating into undamaged bays bounded by stringers on the sides and a frame and tear strap forward and aft to assess the residual strength of the skin and the crack closure effect of the stringer.
- Damage Scenario #3, ST-015 test article: A crack originating from both sides of a fastener hole common to the skin and a stringer propagating into undamaged bays with the underlying stringer severed to assess the residual strength of the skin and multiple element damage.

The fourth damage scenario for residual strength was predetermined for the ST-016 test article by the naturally occurring cracks which existed in the vicinity of the antenna structure.

3.3 Emerging NDI Technologies and SHM Systems

The process of selecting and assessing potential emerging NDI technologies and SHM systems was based upon several criteria. These criteria consisted primarily of cost, sensitivity, false call rate, speed, training requirements, infrastructure requirements, and maturity.

The selected emerging NDI technologies were utilized prior to fatigue testing and residual strength testing to assess the structural integrity of the applicable test article.

One of the requirements for the selected emerging SHM systems was that the installed SHM system would not interfere with required test setup equipment or instrumentation. The SHM systems were incorporated into the fatigue testing to monitor damage progression.

See Sections 8.6 and 8.7 for conclusions and assessments of these technologies.

4 Pretest Analysis Process

Using the results of the detailed inspection procedure conducted by NIAR NDI personnel and the configurations of the damage scenarios, an analytical model of each article was constructed. Each test article was modeled separately to accurately represent the damage configurations. Due to the complexity of the required solid finite element model (FEM) and three-dimensional, mixed mode, stable tearing research code (CRACK3D), NIAR analysis engineers utilized test data to validate the FEM and assess the capabilities of CRACK3D by correlating the analytical “critical crack size” to the full scale testing results. A pretest analysis and prediction program was performed on each article model to predict article failure based on flaw installation and crack growth due to a combination of cyclic and static loads. This prediction was in the form of a critical crack length for each damage scenario and the load required to fail each test article.

A cyclic loading spectrum was developed for the three large panels and was used to initiate and propagate cracks.

5 Development of Test Load and Displacement

Residual strength test loads were calculated using the Lockheed Martin predicted limit stress for the aft fuselage crown skin section at FS 1744 and BL 0.0 of 37.5 ksi. Using the Lockheed Martin drawings and measurements of the test panel widths, the cross sectional area was calculate to be 2.84 square inches.

Using the above information, 100% limit load in an axial loading configuration on the aft fuselage crown skin region at the damage area of interest was the anticipated limit stress multiplied by the cross-sectional area:

100% Limit Load = 37.5 ksi x 2.84 square inches = 106,500 lbs

At the request of TAG team members, limit load was not exceeded during panel testing.

TAG team members also requested that during residual strength testing, test control be by displacement rather than load. To develop a basis for displacement rate, the displacement of the test articles was calculated. The following formula was used to calculate linear displacement of the articles at limit load:

$$\frac{P_{LIMIT} * L}{A * E}$$

where P_{LIMIT} is 106,500 lbs, "L" is the large article length of 114.74 inches, "A" is the cross-sectional area of 2.84 square inches, and "E" is the material modulus of elasticity of 10.3 x 10^6 psi. Based on this calculation, the displacement of the large panels equals 0.4177 inches at 100% limit load. Substituting the length of 73.86 inches for the small panel length in the above formula yielded a small panel displacement of 0.2689 inches. These calculations assumed completely linear elastic material response and were only intended for use in defining a displacement rate during testing.

It was determined from this displacement that a test rate of 0.001 inches per second provided a reasonable overall test time (approximately 7.0 minutes for the large panels and 4.5 minutes for the small panel). These test times allowed time to monitor critical data channels as well as to acquire sufficient data to capture any crack propagation as the loads increased.

5.1 Load Axis

It was desired to load the test article only along its x (long) axis to the maximum extent possible. This was complicated by the fact the test article is saddle shaped (double-curvature) and the stringer area is asymmetric across the test article cross-section.

To minimize bending about the y-axis of the test article in the cross-section containing induced damage for residual strength testing, the distance between the location of applied loads and reaction forces and the neutral axis of bending, or centroidal axis, had to be minimal. To determine the location of this axis, a typical or idealized cross-section was developed. The idealized cross-section was designed based on typical geometry surrounding the defined damage scenarios, which all occurred forward of the start of the saddle (double-curvature) region at FS 1744. Since all damage scenarios were located away from circumferential stiffening members (frames and tear straps), the idealized cross-section only contained the skin and longitudinal stiffeners (stringers). Localized geometric features, such as the antenna supports and personnel restraint system, were not included in the typical cross-section.

The centroid of the test article was calculated based on this idealized cross-section. The test panel centroid did not correspond to the circumferential center of the panel due to asymmetrical stringer area distribution. Stringer 96, a skin splice stringer, had a significantly larger cross-sectional area than the other stringers, and since it was located at the edge of the panel, the test panel centroid was skewed toward stringer 96. Since two hydraulic loading cylinders were used to apply test loads and four reaction links provided the reaction loads, the test article was divided along the test panel centroid into two halves (left/right). The centroid of each half was calculated to determine the location of each loading cylinder. This exercise was repeated by dividing each of the previous halves to determine the ideal location of each of the four reaction links. Figure 8 shows a plot of the calculated locations of each of the load cylinders and reaction links. A quadratic curve fit was used to determine the location of the neutral axis, which formed a nearly circular arc with a radius 0.453 inches less than the radius of the test panel outer mold line (OML). All edge distances were checked, and it was determined that to maintain an edge distance of twice the connection hole diameter, the outer two reaction links would need to be

moved inward on the panel along the centroidal axis.

The 0.453 inches inside the OML dimension allowed for constant thickness buildups in the load and reaction attachment reinforcements on the panel ends. Figure 8 shows the relationship between the actual article centroid, and the locations of the load and reaction points on the test article cross-section. Figure 8 also shows the test article cross-section geometry, load and reaction point locations, reference notes, dimensions, and coordinates.

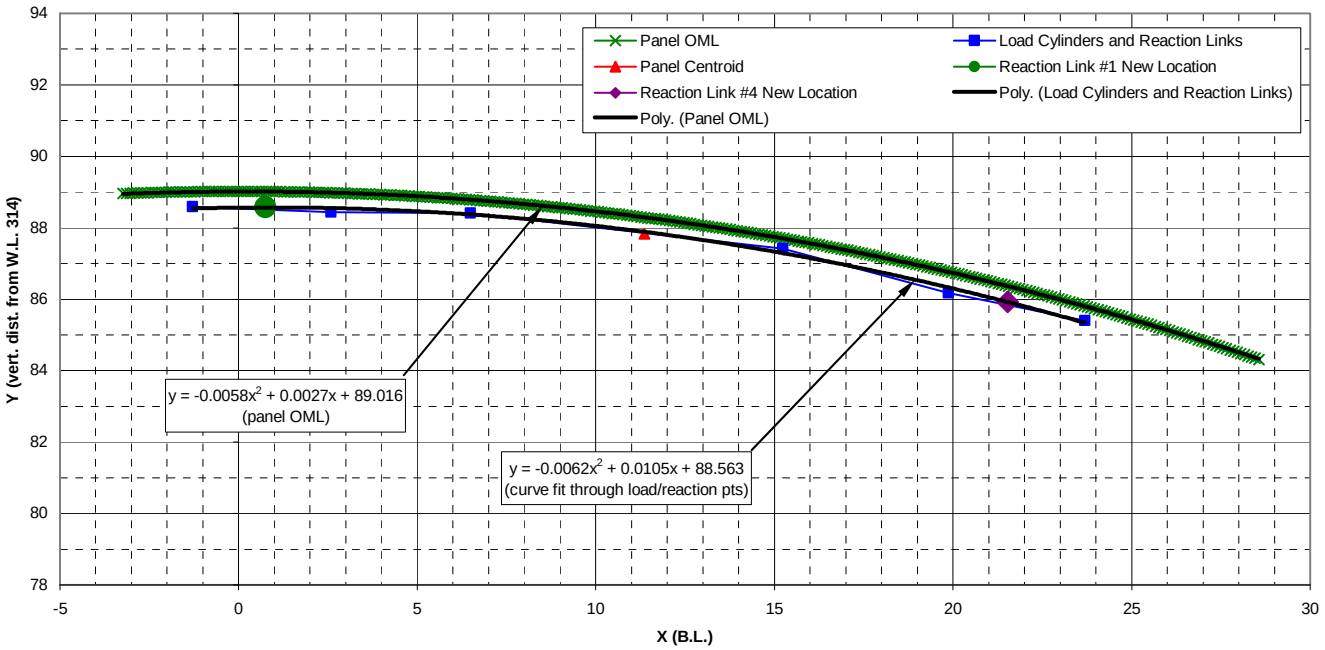

Fig. 8. Test panel centroid vs. load and reaction point locations

5.2 Cyclic Spectrum Development

To transition the induced saw cuts in test articles ST-013, ST-014, and ST-015 to sharp cracks, a variable amplitude (marker band) spectrum was incorporated into the otherwise constant amplitude spectrum. Cracks were propagated from the initial induced damage state to a length which would induce panel cross-sectional failure at or below the residual strength limit load magnitude (some size beyond the estimated critical crack length of 2.77 inches). This spectrum used changes in the maximum applied load to create marker bands on the fracture surface. This marking of the crack face enabled a correlation of crack length to cycle count post failure by fractographic analysis. Figure 9 shows the 10-4-6 marker band pattern selected for this program. This spectrum has an R ratio (minimum stress/maximum stress) of 0.05. The areas of reduced stress in the marker band region have a maximum stress value of 80% of the maximum stress of the 2,000 cycle region. AFGROW, a linear elastic fracture mechanics software, was used to predict the number of cycles required to grow the crack from the initial damage state to lengths beyond the anticipated critical crack length of 2.77 inches at various stress levels. This analysis does not account for the number of cycles required to transition the blunt saw cut (0.005 inches wide) to a sharp fatigue crack.

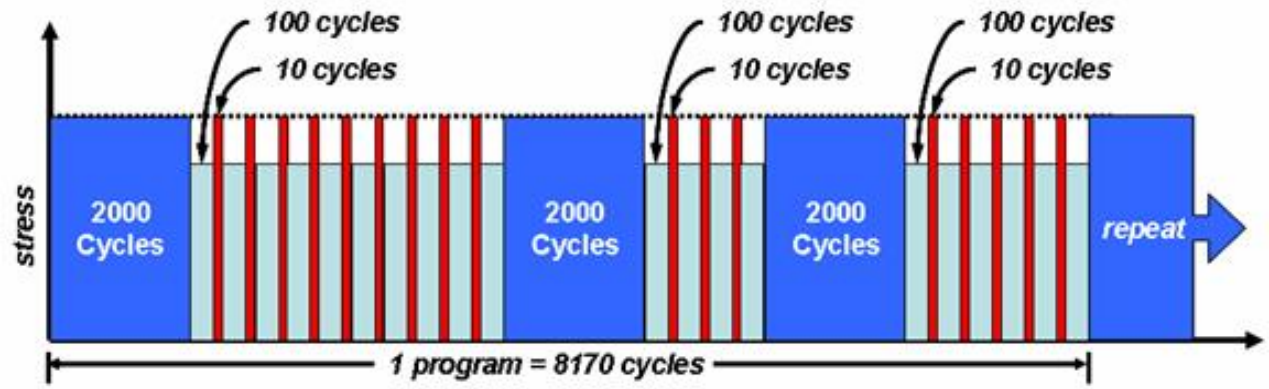

Fig. 9. Marker band cyclic spectrum diagram

`

The unstiffened skin of the C-5A test article was modeled in AFGROW and the Walker equation was used to predict crack growth rates. To determine the maximum stress value in the marker band spectrum, stress multiplication factors were implemented to find a value capable of propagating the crack at a rate that would allow ample inspection opportunities between desired crack growth increments. The desired crack growth increment between static tests was determined by the size of the plastic zone. It was desirable to propagate the crack tip through the plastic zone that resulted from the previous static limit load application (monotonic plastic zone). An Irwin approximation was used to predict the monotonic plastic zone size following each application of displacement corresponding to limit load. Since the skin of the test article was 0.050 inches thick, the skin was assumed to be in a state of plane stress. Therefore an index value of two was used in the Irwin approximation. The closure retardation model was also used in the crack growth calculations.

A stress multiplication factor of eight and a resulting maximum stress of 8 ksi was selected for the fatigue spectrum. Table 1 shows the crack lengths that were subjected to static loading, the predicted number of cycles required to reach these crack lengths, the stress intensity factor (SIF) corresponding to the fatigue loading, Irwin approximations of the plastic zone size due to fatigue loading, the SIF corresponding to the static limit load applied at these crack lengths, Irwin approximations of plastic zone size due to static loads, and the selected crack growth increments.

Table 1. Fatigue crack growth intervals

Crack Length (in)	Total Number of Fatigue Cycles	SIF Fatigue Loading (ksi√in)	Cyclic Plastic Zone Size (in)	SIF Static Loading (ksi√in)	Monotonic Plastic Zone Size (in)	Crack Growth Increment per Tip (in)
0.90	0	9.51	0.0029	---	---	0.05
1.00	7493	10.03	0.0033	47.00	0.07	0.13
1.26	22772	11.25	0.0041	52.76	0.09	0.13
1.52	33266	12.36	0.0050	57.96	0.11	0.13
1.78	41116	13.38	0.0058	62.73	0.13	0.13
2.04	47092	14.32	0.0067	67.16	0.15	0.15
2.34	49133	15.34	0.0076	71.93	0.17	0.215
2.77	58340	16.69	0.0090	78.22	0.20	0.20
3.17	62786	17.85	0.0104	83.75	0.23	0.23
3.63	66306	19.10	0.0119	89.64	0.26	0.27
4.17	69899	20.47	0.0136	96.11	0.30	---

5.3 Inspection Intervals and Procedures

Inspection intervals were also developed based on this information. Table 2 shows the inspection intervals during the cyclic testing for each increment of crack growth. These intervals are roughly based on 50%, 75%, 90%, and 95% of the number of cycles required to propagate the crack through each crack growth increment.

It should be noted that these inspection intervals changed due to rate of crack growth. Actual inspection intervals during testing were documented.

The following inspection procedure was used during each inspection interval to examine the test article:

Table 2. Inspection intervals

Crack Length (in)	Number of Cycles Inspection 1	Number of Cycles Inspection 2	Number of Cycles Inspection 3	Number of Cycles Inspection 4
0.90	---	---	---	---
1.00	3,750	5,600	6,750	7,250
1.26	15,100	19,000	21,250	22,500
1.52	28,000	30,750	32,000	33,000
1.78	37,000	39,000	40,000	41,000
2.04	44,000	45,500	46,500	47,000
2.34	48,000	48,600	49,000	No Inspection
2.77	53,750	56,000	57,000	58,000
3.17	60,500	61,500	62,000	62,500
3.63	64,500	65,500	66,000	66,250
4.17	68,100	69,000	69,500	69,750

5.3.1 Inspection Procedure

1. Inspected induced flaw area using ECSS inspection to document condition of flaw ends and growth (if any) of cracks propagating from flaw ends.
2. Visually inspected local area around the induced flaw, area to include stingers, strap, and frame flange bounding the bay in which the induced flaw was installed.
3. Inspected previously documented existing cracks in test article (if any) using ECSS inspection methods. Documented the growth (if any) of existing cracks.
4. Inspected NDI/SHM installed flaw using ECSS inspection to document flaw length and growth (if any) of cracks propagating from flaw end.
5. Visually inspected areas of installation of end reinforcement buildups at both ends of the test article, particularly in the area inside the frame flanges under the outer reinforcement doubler at each end.

All inspections and results were documented. Crack lengths were recorded and tracked.

5.4 Cyclic Test Loads Definition

Based on the 8 ksi maximum stress level, the 80% stress reduction for the marker band reduced loads (6.4 ksi), and a minimum stress equaling 5% of the maximum stress level (0.4 ksi), test loads were calculated based on the 2.84 square inch area of the test article at the area of interest. The resulting cyclic test loads (maximum, reduced, minimum) are presented in Table 3.

Table 3. Test article cyclic test loads

Load Description	Stress (ksi)	Total Load (lbs)	Load per Cylinder (2 ea) (lbs)
Maximum (2,000 & 10 cycle blocks)	8.0	22,720	11,360
Reduced (100 cycle blocks)	6.4	18,176	9,088
Minimum (all blocks)	0.4	1,136	568

5.5 Residual Strength Test Loads and Predicted Failure Loads

Predicted failure load magnitudes were based on the inspection results and Lockheed Martin failure prediction methods. These were used only as a guideline for anticipated failures during residual strength testing.

6 Test Setup

The test articles were assembled to forward and aft boundary fixtures and this assembly was installed in a reinforced stand alone test fixture. Strain gages and displacement transducers were installed on the test article to monitor strain and displacement of the test article during testing. Loading systems utilizing hydraulic fluid power were installed on the test article/boundary fixture assembly to apply test loads to satisfy the requirements for this test program. SHM systems were also installed for the test program. A load control system (LCS) and data acquisition (DAC) system were configured and calibrated to apply/control test loads and record data during testing.

6.1 Load Application and Reaction Feature

Due to the magnitude of the 100% limit load and the predicted failure loads, the test load was distributed along the circumferential direction of the panel in two equal load distributions at two locations for the "active" load inputs, and at four locations for the "reaction" loads. The active test loads were applied at the aft edge of the test article through the aft boundary fixture. The reaction/anchor loads were reacted into the test fixture through the forward boundary fixture. Each test load was located at the centroidal cross-section of the test panel as described in Section 5.1. Cyclic and residual strength test loads were applied at the same locations. Table 4 presents the test panel active and reaction load descriptions for all panels.

Table 4. Test panel load descriptions

Test Load ID	Reaction Load ID	Test Load Location Description
P1		Inboard – Active
P2		Outboard – Active
	R1-1	Inboard Load – Inboard Reactive
	R1-2	Inboard Load – Outboard Reactive
	R2-1	Outboard Load – Inboard Reactive
	R2-2	Outboard Load – Outboard Reactive

Forward and aft boundary fixtures were designed and fabricated to provide a means of attachment to the test panel to transfer test and reaction loads through the test panel in an evenly distributed manner across the cross-section of the test article.

The design of the boundary fixtures were based on previous test programs performed on stringer test sections by LM Aero at the Marietta Georgia test facility. Test panel loads were calculated based on the desired gross area stress in the damage region. An existing Lockheed Martin design was used for end pad reinforcement. The boundary fixture was fabricated from aluminum plate and sheet.

The boundary fixture was fabricated so that the assembly of the fixture to the test panel allowed applied and reaction test loads to represent panel loading as installed in the aircraft as closely as possible. The fixture was attached on both sides of the panel skin, with attaching/ assembling hardware in double shear configuration. The test and reaction load attach points were located based on centroidal area calculations of the panel cross-section containing damage to represent a uniformly distributed load across the test article in the region containing damage.

6.2 Tare Weight Systems

Because the test article orientation during testing was with the x – axis parallel to the floor, two separate tare weight systems were utilized: a test article/boundary fixture tare weight system and a loading system tare weight system.

The test article and boundary fixture weight was neutralized by a tare weight system which

lifted the weight of total test panel assembly at four locations. Canvas loop patches (16.5 square inch areas) were bonded to the test article at stringer/frame intersections that were located away from the area of interest. These locations were connected to a whiffletree distribution system that resolved to a single lift point, which was the theoretical center of gravity of the test article. The whiffletrees connected to the lift point with strap or cable, and a length of cable at the lift point ran up and over two pulleys and down to a weight pan. Lead weights or shot bags representing the total weight of the test article and tare system were placed in the weight pan.

The weight of the loading and reaction link systems was neutralized by a tare weight system consisting of three whiffletrees that lifted the weight of the systems. Each loading cylinder had its own lifting whiffletree and the weight of the four reaction links were supported by a whiffletree. The whiffletrees were connected to the lift point with strap or cable, and a length of cable at the lift point ran up and over two pulleys and down to a weight pan. Lead weights or shot bags representing the total weight of the attached loading systems and tare system were placed in the weight pan.

6.3 Instrumentation

The instrumentation requirements for each panel were developed based on recommendations of the TAG team members from previous test programs, stress analysis, and previous inspection/damage sites. The results of the NIAR NDI program also served as a basis for instrumentation definition based on documentation of existing damage indications.

Test instrumentation was defined to monitor the article during testing. Calibrated dual bridge load cells were installed to monitor the test load as part of the test control loop on the hydraulic load cylinders attached to the aft boundary fixture on the test article. Linear displacement transducers (LDTs) were installed parallel to the cylinder for stroke control during residual strength load applications. Calibrated load links were installed on the forward boundary fixture to provide reaction loads. Strain gages and displacement transducers were utilized in selected locations to provide data during testing.

Following testing of the ST-013 test article, additional strain gages were added to monitor the splice area of the test article during testing.

Approximately 60 channels of strain gages were installed in critical locations that required strain monitoring during testing. The type of gage (axial, rosette, etc.), size of gage, and strain range was defined for each location based on previous test program results, pretest analysis finding, or other data sources pertinent to this program.

Displacement transducers were installed in critical locations to monitor overall article displacement and motion in the three main axes as well as to monitor fixture motion.

Load cells purchased from Tovey Engineering were used for load feedback for control and monitoring. Prior to testing, all load cells were calibrated and certified by Tovey Engineering using quality assurance procedures that were traceable to standards established by the National Institute of Standards and Technology (NIST). Load cell calibration documentation was maintained by Tovey Engineering and was provided to NIAR.

The four reaction links were fabricated from 7075-T6 aluminum and had full bridge strain gage configurations installed. The links were calibrated in tension load for reaction load monitoring during testing. A ten point calibration from zero to 70,000 lbs was performed on each link. The link end that attached to the test article was slotted to allow loading cylinder travel to fully extend without placing the article in compression.

6.4 LCS, DAC, and Hydraulic Systems

The test loads were applied using MTS® AeroST with AeroPro software. It had all of the standard system monitoring features such as loop error, load limits, time ramp functions, tare function, Proportional-Integral-Derivative (PID) loop, 8-wire with excitation monitoring, etc.

Test article loading was achieved using two methods. The static (residual strength) portion was stroke (displacement) controlled utilizing

two linear variable displacement transducers (LVDTs) mounted on each hydraulic cylinder as the feedback loop. The dynamic or cyclic portion of testing was run using load control and utilized two Tovey 200K lb load cells as the feedback loop. During residual strength testing, the load cell signals were monitored even though they were not controlling.

To ensure the correct load was being applied, two independent systems, LCS and DAC, were separately set up using calibration data from an independent metrology laboratory for each load cell and LVDT. In addition, an external Shunt (RCal) resistor was applied at the load cell to ensure the DAC was reading correctly. Each hydraulic cylinder was then put into a captive fixture and run up to the maximum load for the test and the load data from each system was compared.

Hydraulics were controlled by the MTS® AeroST. Upon command from an operator, the MTS® AeroST opened a shutoff valve and closed a bypass valve to allow hydraulic oil to flow. Hydraulic pressure was manually adjusted from zero to operating pressure by an operator. The MTS® AeroST was set up to remove hydraulic pressure from the test setup by actions triggered as a result of specific errors that were monitored during testing.

Test load intervals, load ramp times and sequences, test load tolerances, and the DAC system recording intervals were preprogrammed prior to testing.

The DAC system that was utilized during testing was a VXI 1629. It is integrated into the MTS® AeroPro software so all of its screens were available from the same system for set up and monitoring. The DAC is a 16-bit system using four-wire transducer wiring. The sample rate for the DAC during testing was set at twenty samples per second for both manual and continuous data recording.

Data was exported in ASCII format and compatible with Microsoft® Excel® spreadsheet software for data reduction and analysis.

The DAC had a real-time display with the following types of display windows available:

- Real-time Display: Tabular list of channels, XY plots, strip charts, bar charts.
- One client computer
- Computed (calculated) channels were available

Hydraulic power was provided by a 60 gallon per minute (gpm) hydraulic pump. The flow and pressure of the hydraulic fluid was regulated to the test loading systems through an isolator test panel installed at the test fixture.

6.5 Incorporation of SHM Systems into Test Setup

A set of criteria for SHM selection was determined by the TAG team members. Based on the results of the selection process, two SHM techniques were incorporated into the fatigue and residual strength tests of test articles ST-014 and ST-015.

Consideration was given to each SHM system and its requested locations for sensors with respect to strain gage and LDT locations.

7 Test Procedures

After the test article is installed in the test fixture and test instrumentation is installed, the following pretest and test procedures will be utilized for the ST-013 test article. Based on the results of the ST-013 testing, the procedures may be modified for subsequent article testing.

7.1 Pretest Procedure

1. Test setup photographs will be taken.
2. Using a displacement control command/feedback loop, the test article will be loaded to 40% limit load (by monitoring the load cell feedback channels) at the predetermined displacement rate of 0.001 inches per second. Loading will be paused at 5% limit load increments and data recorded.
3. Using the displacement command/feedback loop, reduce test load on the article to 0% load in 10% increments at the same displacement rate.

4. After the 40% pretest run, at the discretion of project personnel present, the test article may be loaded to 60% limit load using the same pretest procedure.
5. Install induced flaw per Damage Scenario #1.
6. After flaw has been installed and approved, proceeded with the following cyclic test procedure.

7.2 Cyclic Test Procedure

1. Using load control, the test article will be loaded to the "tare" load condition (test article and boundary fixture/load linkage weights supported by tare weight systems).
2. All strain gage and displacement transducer channels will be zeroed and a brief data scan will be recorded.
3. Test setup photographs will be taken.
4. The test article will be loaded to the maximum amplitude load level of the cyclic spectrum (see Table 3) and an instrumentation and equipment check will be conducted, including strain and displacement checks. A brief data scan will be recorded at the initial maximum amplitude load level.
5. After equipment and data checks, cyclic spectrum testing will commenced. Data scans of test instrumentation will be recorded during each occurrence of the 2,000 cycle load block, one at the beginning of the block and one at the end. Approximately ten cycles of data will be recorded during each scan.
6. Testing will be stopped at a predetermined cycle interval for NDI (see Table 2).
7. If natural cracks have not propagated to the required length (see Table 1), the test will be restarted.
8. Steps 6 and 7 will be repeated until a predetermined cycle count is reached, or when crack(s) reach a predetermined "test" length.
9. The test article will be subjected to NDI procedure described in Section 5.3.1.
10. Conduct residual strength testing.

7.3 Residual Strength Test Procedure

1. The test article will be loaded to the "tare" load condition (test article and boundary fixture/load linkage weights supported by tare weight systems).
2. All strain gage and displacement transducer channels will be zeroed.
3. Test setup photographs will be taken and test video (if utilized) equipment will be prepared for video start at approximately 80% limit load.
4. The DAC will be configured and a zero load data scan will be recorded.
5. The test will start using displacement (stroke) control at a constant displacement rate of 0.001 inches per second. The MTS® data system will record data in a continuous mode of one sample every four seconds. This displacement rate and data capture method will be utilized until the test reaches 80% limit load.
6. At the 80% limit load level, the test stroke control will be slowed to a constant rate of 0.0001 inches per second. The MTS® data system will transition to a scan rate of ten samples per second.
7. Loading of the test article will continue at a continuous ramp rate of 0.0001 inches per second until the test article fails, or to 100% limit load and held for three seconds.

<u>If 100% limit load is achieved without test article failure, proceed with Steps 8a – 11a:</u>

8a. Reduce the test displacement to zero using a displacement rate of 0.002 inches per second. MTS® data system will record continuous data scans at the rate of one scan per two seconds.

9a. Hydraulic pressure will be removed from the test article.

10a. After testing is complete, conduct a thorough NDI procedure (see Section 5.3.1), documenting the condition test article, include the condition of the induced flaw and natural cracks.

11a. Reconfigure the test setup for cyclic testing, and repeat procedure per Section 7.2.

If test article failure occurs at or below 100% limit load, proceed with Steps 8b – 10b.

8b. Hydraulic pressure will be removed from the test article.
9b. Visual inspection will be conducted on the test article in the "as is" condition.
10b. The test panel will be removed from the test fixture and subjected to a teardown examination and inspection program.

8 Test Results Summary – Test Articles

The following summaries discuss the testing and results of ST-013 through ST-016 test articles.

8.1 Test Article ST-013 Test Summary and Results

ST-013 was the first skin panel section tested and basically resulted in being a development tool for establishing the test procedures for the remaining test articles. The test article was mounted in the test fixture as shown in Figure 10.

Fig. 10. ST-013 test article in test fixture

A series of low level static tests were conducted to verify that the loading system would accurately and repeatedly produce the desired loads in the test area of the panel. The results of this testing were very positive and showed that the axial loads induced in the panel produced nearly constant and repeatable strains across the panel with very low levels of bending based on the strain gage data. As a result, the TAG team members agreed to proceed with the installation of the test flaw.

The flaw induced in the ST-013 article was a 0.350 inch circumferential cut centered between stringers 91 and 93 at FS 1729. This was accomplished by drilling a #40 hole at desired location and then cutting 90º to the stringers an equal distance to achieve the proper overall centered length. Figure 11 shows the initial installation of the flaw.

Fig. 11. ST-013 flaw initial installation

The general test plan was to grow a crack from the flaw location in increments of 0.500 inches overall flaw size (induced flaw plus natural crack) using cyclic loads and then run a static load test to limit load. This process was to be repeated at predetermined crack lengths until the article failed at or prior to limit load.

Analysis showed that a peak stress level of 8 ksi should be used during cyclic testing to achieve the desired crack growth rate from the induced flaw. The test article was loaded statically to determine the proper test load that would yield the desired stress based on the strain levels.

Cyclic testing was then started at this test load of 28,750 pounds (8 ksi). Figure 12 shows the cyclic test setup.

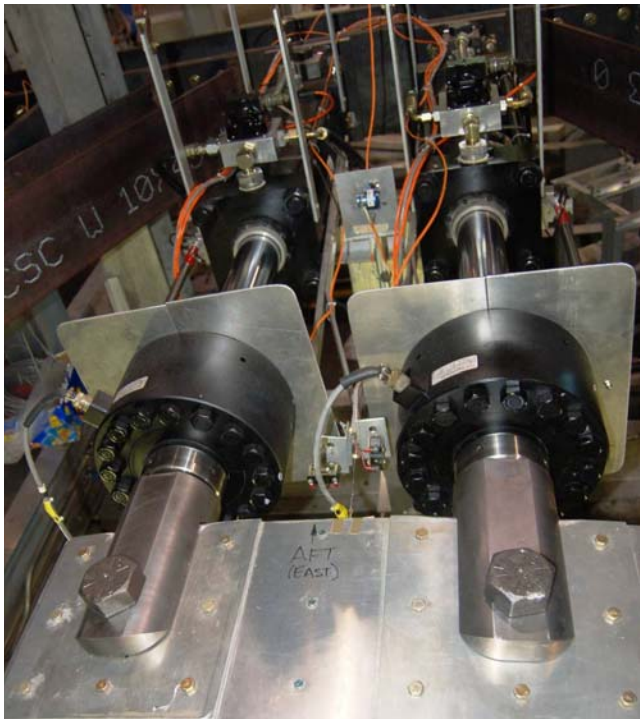

Fig. 12. ST-013 cyclic test setup

Inspection of the article was performed approximately every 12,000 cycles to monitor the crack growth from the ends of the induced flaw. No crack growth was detected from the flaw until the inspection at 60,000 cycles at which point a crack growth of 0.043 inches was noted on the inboard end of the flaw. Inspection intervals were then reduced to every 2,500 cycles. This crack continued to grow slowly with no growth from the other side of the flaw until 90,000 cycles had been completed at which point the inboard side measured 0.115 inches and a crack of 0.023 inches was detected on the outboard side. At 92,500 cycles an overall flaw length of 0.533 inches was reached and the first limit load test conducted.

The panel held limit load of 106,500 pounds with no apparent problems. Post test inspection revealed that the overall flaw length had grown to 0.583 inches during the limit load condition.

Cyclic testing was then resumed and cycled from 92,500 cycles to 192,500 cycles with no detectable crack growth from the flaw. At this point it was theorized that the crack tips had plasticized during the limit load testing. After consultation it was then agreed between the TAG team members to increase cyclic load from 28,750 (8 ksi) to 54,000 pounds (15 ksi). Testing resumed at this load to 213,771 cycles at which point a crack growth of 0.021 inches was noted on the outboard side of the flaw. No growth was detected on the inboard side. Testing then continued to 216,500 cycles at which point the crack had grown from both sides of the flaw to an overall length of 0.649 inches which was the next point established to conduct a limit load test.

At 87,081 pounds, approximately 82% of limit load the panel completely separated along the production splice at FS 1744 which was 15 inches forward of the flaw area. Following this event, sections of the panel along the failed area as well as the flaw area were removed and sent to CAStLE for fractographic analysis. To summarize, it was found that during the extended period of cyclic loading with no crack growth at the flaw site, which was then followed by additional cyclic loading at the significantly increased load to get the induced flaw to continue growing, numerous cracks had initiated from the fasteners along the skin splice. These cracks had extended down into several of the stringers along the splice and were visually undetectable. Significant review and analysis of the failure and test methods used were conducted by NIAR and discussed with the other TAG team members to determine “a way forward” with the remaining test panels. From the findings of these reviews, several modifications to the test methods were made for the following panels. The most notable was to increase the initial flaw size and to mechanically cut through the plasticized region of the induced flaw cracks after limit load test conditions. Both changes were aimed at reducing the number of fatigue cycles that the overall test article would be exposed to.

8.2 Test Article ST-015 Test Summary and Results

ST-015 was the second panel tested. The article was mounted in the test fixture similarly to the ST-013 test article and initial strain surveys completed with good results. At this point, an enhancement was made to the test procedure as a result of the ST-013 data review: the load

distribution between the two load cylinders was biased to produce equal displacement across the panel at a given test load.

This was needed due to the difference in the cross-sectional area of the panel at stringers 87 through 91 as opposed to stringers 93 through 96. The amount of bias was determined by loading the article to the peak cyclic load value and then adjusting the loads to produce equal displacements. The percentage of bias was recorded and incorporated into the load control programming. The load was then reapplied to verify that with the bias incorporated that the proper displacement and total load was achieved.

Since panel ST-013 had not provided the needed center panel crack growth information (it failed away from the induced flaw), it was decided to change the flaw location on ST-015 to the same location as ST-013 which was a circumferential cut centered between stringers 91 and 93 at FS 1729. The initial installed flaw length target was 0.500 inches. The actual installed flaw length was measured as 0.501 inches. Ladder type crack detection gages were installed near the crack tips as a monitoring device to ensure that cracks did not grow excessively without being noticed. Cyclic testing was then started using the 8 ksi load level.

At 6,358 cycles the crack gages indicated that the natural cracks had initiated. The flaw was inspected and it was verified that natural cracking had initiated at both ends of the flaw. The outboard side had grown 0.062 inches and the inboard side had grown 0.055 inches for a total flaw size of 0.618 inches. This approximated the desired length for the first test damage condition of 0.625 inches and it was decided to proceed with the first residual strength test.

The test system was converted to the static test setup and the test loads were applied similar to the procedure used on ST-013. The panel was able to hold the limit load of 106,500 pounds with no noted issues. The flaw as well as the overall panel was then inspected. There was no measured growth of the crack at the flaw location and no damage noted. The outboard end of the flaw did show evidence of the chevron effect indicating plasticizing of the crack ends. The flaw was then mechanically lengthened to an overall length of 0.738 inches, with the goal of extending the flaw tips through the crack-retarding plastic zones. The test setup was then converted back to cyclic test and testing resumed.

The flaw in the panel was inspected at approximately every 2,500 cycles and cycled to 49,029 cycles with no appreciable crack growth. It was assumed at that point that the flaw had not been lengthened enough to get past the plasticized area. It was then agreed by the TAG members that the flaw would be mechanically extended another 0.060 inches. The new overall flaw size measured 0.868 inches.

At 52,110 cycles crack growth was evident at both ends of the flaw and at 52,358 cycles had reached an overall length of 0.973 inches which was just past the next length set for a residual strength test.

The residual strength test was conducted and the panel again was able to hold the limit load value without incident. The post test inspection of the flaw showed that the flaw had extended 0.021 inches during the limit load application to an overall flaw size of 0.994 inches.

The flaw was then mechanically extended to a total length of 1.255 inches with the next residual strength test point being 1.354 inches. Inspections were set for every 500 cycles and testing resumed.

At 56,040 total cycles the flaw had grown to an overall length of 1.360 inches and the test setup converted back to residual strength testing. Limit load test #3 was completed with the panel again holding the limit load level with no anomalies. Post test inspection again showed that the flaw had grown 0.031 inches to an overall flaw size of 1.391 inches. Both ends of the flaw showed evidence of the chevron effect.

The flaw was then mechanically extended to an overall length of 1.711 inches and the next residual strength test planned for 1.811 inches overall flaw size. Cyclic testing was resumed and after an additional approximately 5,500 cycles (63,710 total cycles) had shown no crack growth. Testing was stopped and the flaw

mechanically extended approximately 0.050 at each end to a new total length of 1.810 inches and the new residual strength test point set for 1.911 inches. Testing continued to 66,710 cycles when inspection showed that the cracks had extended the flaw to an overall length of 1.900 inches.

Residual strength test #4 was then conducted and the panel was able to withstand limit load with no apparent issues. Post test inspection revealed the flaw had grown 0.091 inches during the test to a new overall length of 1.991 inches. The overall flaw length was mechanically increased to 2.441 inches and the next residual strength test set for 2.541 inches. Cyclic testing was continued for 3,740 additional cycles. Since no crack growth was noted during this time, it was decided to mechanically lengthen the flaw to a new overall length of 2.670 inches and the next residual strength test set at a length of 2.770 inches. Cyclic testing was resumed at 70,450 cycles and continued to 71,630 when inspection indicated that the overall length was 2.770 inches.

Residual strength test #5 was then conducted. During loading at 73% and again at 86% of limit load, small pops were heard from the test article. At 97% of limit a louder pop was heard. The load continued to the limit load value and the panel continued to hold load. The post test inspection revealed that the flaw had extended to the fasteners at stringers 91 and 93. The video of the test showed that the crack had grown at each of the small pops and then run to the stringers at the louder pop where the crack was arrested and the panel was still capable of holding increased load. During the post test inspection the overall flaw was measured as 5.884 inches. A photo of the flaw after residual test #5 is shown in Figure 13.

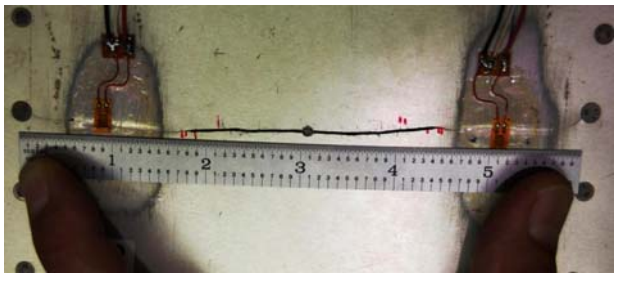

Fig. 13. ST-015 flaw after limit load test #5

NIAR consulted with the other TAG team members on how to proceed with testing. It was decided to mechanically extend the flaw 1.000 inch past the fasteners at stringers 91 and 93 in the skin only and then cyclic load to start natural cracks and repeat the residual strength test when the overall length reached 8.200 inches.

The flaw was extended and measured 8.097 inches before starting cyclic loading. Cyclic testing was started with inspection every 100 cycles until crack growth was noted and then shortened to every 50 cycles. At 550 cycles the crack had grown to 8.201 inches and the setup was converted to the residual strength test. The panel flaw at this point is shown in Figure 14.

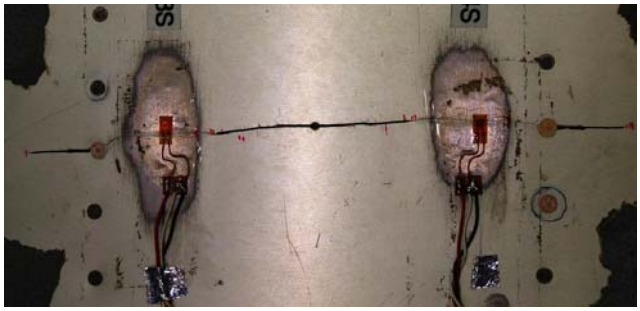

Fig. 14. ST-015 flaw prior to limit load test #6

During application of the residual strength test loads, small pops were heard at 26%, 68% and 74% of limit load. At 78.4% (83,464 pounds) the panel separated along the flaw area as shown in Figure 15.

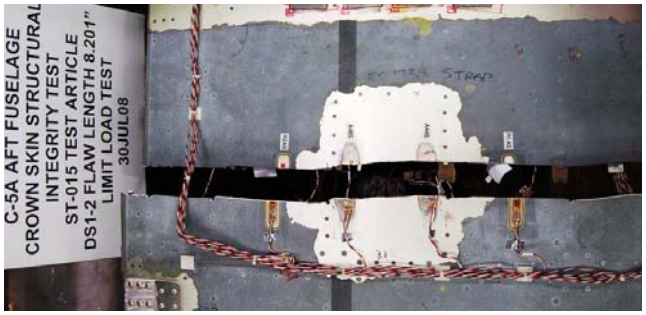

Fig. 15. ST-015 flaw separation after limit load test #6

The panel was removed from the test fixture and small sections forward and aft of the failure region were cut from the panel and sent to CAStLE for fractographic analysis. All areas along the failure point including the stringers, other than the flaw area as previously described, showed only overload failures. This validated the method of mechanically extending cracks

through the crack tip plastic zones to avoid unnecessary fatigue cycling.

8.3 Test Article ST-014 Test Summary and Results

Test article ST-014 was the third panel tested. The test article was mounted in the test fixture similarly to the previous panels and initial strain surveys were completed with good results. The cyclic load level of 8 ksi was used and the load distribution biased similar to test article ST-015 to maintain equal displacement across the panel.

The initial flaw installation for ST-014 was to induce a cut in the skin only, equally on both sides of the fastener located on stringer 93 at FS 1727.8 and with an overall length of 1.400 inches. The target crack length for the first residual strength test was set at 1.50 inches.

Cyclic testing was started and at 936 cycles crack growth was noted. The test was stopped at 1,725 cycles; the overall flaw measured 1.500 inches. The test article and test setup were then readied for the first residual strength testing. The test procedure for the residual strength tests on ST-014 were the same as for ST-015.

The residual strength test was started and progressed without incident until 94% load at which point one of the safety systems within the load control system dumped the test. It was determined that the limits had not been correctly set even though the loading had been proper.

After consultation with TAG team members, it was decided to count the test as valid rather than apply two successive near limit load cycles to the test article and potentially alter the crack growth characteristics. The article was fully inspected and no damage found. There was no growth noted at the flaw location.

The flaw was then mechanically extended to an overall length of 1.900 inches and a residual strength test point set at 2.000 inches. Cyclic testing was resumed and at a total of 4,100 cycles the overall flaw length was measured at 2.060 inches. Setup was then accomplished for the second residual strength test.

The second residual strength test was conducted with no anomalies and the panel held the limit load. A slight increase in the length of the flaw was noted and the overall length measured 2.130 inches.

The flaw was then extended to an overall length of 2.560 inches and the next residual strength test set for 2.660 inches. Cyclic testing was resumed and at the total cycle count of 6,530 load cycles, the desired flaw length was met.

Residual strength test #3 was then conducted. During the test at 61%, 78% and at 97.6% of limit load, small pops were heard coming from the test article. Limit load was reached and held. Post test inspection showed that the flaw had grown to 2.800 inches (0.014 inches) during the test. No other damage was noted.

The flaw was then mechanically extended to an overall length of 3.390 inches and the next residual strength test set for 3.500 inches. Cyclic testing was resumed until a total of 8,280 cycles were completed at which point the desired flaw length had been reached.

Residual strength test #4 was then conducted successfully to 100% of limit load. A small pop was heard from the test article at 97% of limit load. The post test inspection revealed that the flaw had grown 0.700 inches to an overall length of 4.280 inches.

The flaw was then mechanically extended to an overall length of 5.080 inches and the next residual strength test set for 5.180 inches. Cyclic testing continued until a total of 8,770 cycles were completed at which point the flaw length had reached 5.206 inches as shown in Figure 16.

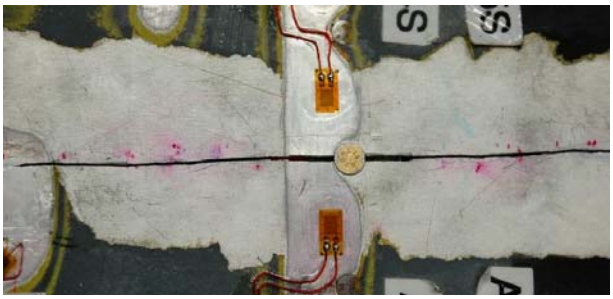

Fig. 16. ST-014 flaw prior to limit load test #5

Residual strength test #5 was then conducted on test article ST-014. Testing proceeded normally and small pops were heard

at 81.8% and at 82.5%. Then at 88.6% (94,378 pounds), the test article separated circumferentially along the flaw as shown in Figure 17.

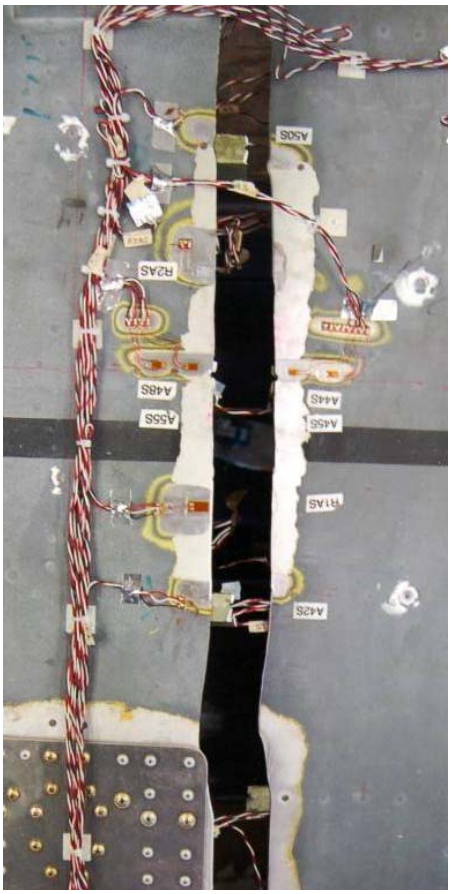

Fig. 17. ST-014 flaw separation after limit load test #5

Similar to ST-015, small sections forward and aft of the failure region were cut from the panel and sent to CAStLE for fractographic analysis. All areas along the failure point including the stringers, other than the flaw area as previously described, only showed overload failure.

8.4 Test Article ST-016 Test Summary and Results

Test article ST-016 panel was cut shorter than the other panels due to a skin repair that had been performed on the aircraft, during service, aft of FS 1744 which had used a different type of aluminum than the production configuration and was undesirable to include in the testing. Therefore, only the area forward of FS 1744 was utilized for the testing of the ST-016 test article.

The test plan for ST-016 was to conduct a residual strength test only on naturally existing cracks located near the antenna cutout at FS 1704 and between stringers 91 and 93. There were three natural cracks as shown in Figure 18. Crack 1 is an off-axis crack 2.230 inches long. Crack 2 is an off-axis crack 2.570 inches long. Crack 3 is an off-axis crack 0.650 inches long.

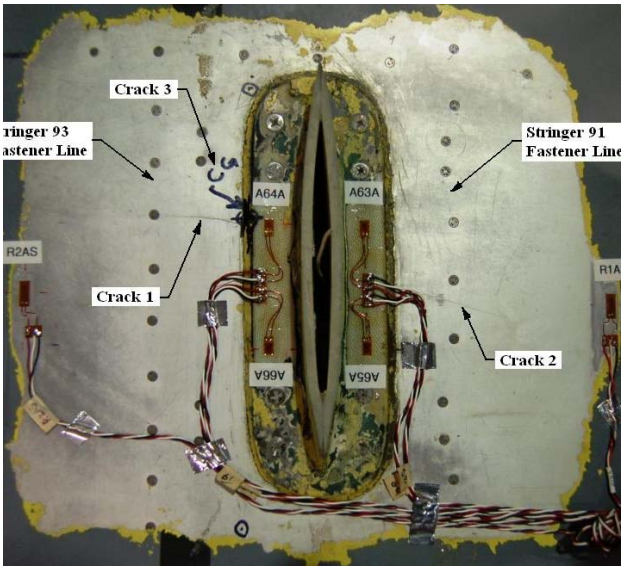

Fig. 18. ST-016 flaw (cracks 1, 2, and 3) prior to limit load test #1

The test fixture and setup for test article ST-016 was the same as for test article ST-014 except a section was added to accommodate the shorter length of the article.

Initially, a strain survey was conducted on the panel with a 10,000 pound load to verify the loading system was inducing load into the panel properly. The strain survey showed that the strains were similar to those measured on the previous test articles at that load level.

The residual strength test was then conducted using the same procedures as for previous test articles. The test progressed normally to 87.7% of limit load when a loud pop was heard coming from the test article followed by a louder pop at 89% limit load. The test article maintained load and successfully reached limit load. Post test inspection revealed that crack 2 had grown to a fastener common to the skin and stringer 89 where the crack had been arrested as shown in Figure 19. Crack 2 had grown from the original 2.380 inches to

7.210 inches. Cracks 1 and 3 did not show any crack growth.

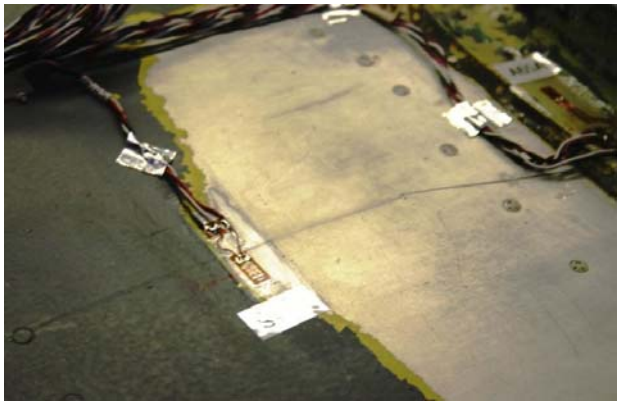

Fig. 19. ST-016 flaw crack 2 after limit load test #1

After discussion with the TAG team members it was decided to modify the test plan to mechanically extend cracks 1 and 2 past the fastener 0.100 inches, apply cyclic loads until natural cracks initiated, and then repeat the residual strength test.

Cyclic testing was then conducted and after 4,700 cycles no crack growth had been detected. It was then decided to extend the cracks an additional 0.500 inches. The crack lengths were now 2.420 inches for crack 1 and 7.950 inches on crack 2. The fasteners that the cracks ran through were also left out to provide more stress at the crack tips, see Figure 20.

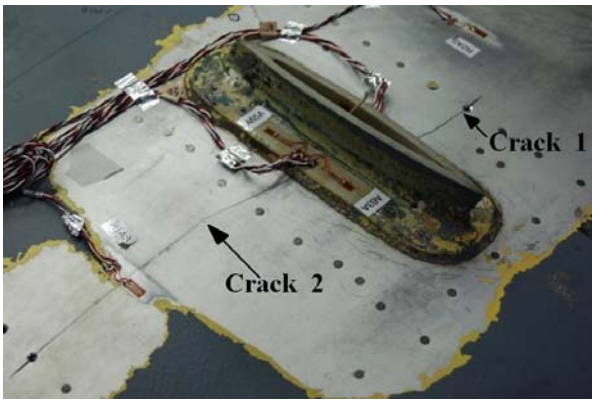

Fig. 20. ST-016 flaw cracks 1 and 2 mechanical extensions at 4,700 cycles

Cyclic testing was continued to 5,450 cycles at which point both cracks had shown a growth of approximately 0.030 inches. Crack 1 was documented at 2.447 inches and crack 2 at 7.970 inches.

The fasteners that the cracks ran through were reinstalled and the test setup changed over to residual strength test loads. The loads were applied as with previous residual load tests. The test progressed normally to 60% of limit load when noises were heard from the test article and continued as the load increased. At 69.2% of limit load the article separated circumferentially through the cracks as shown in Figure 21.

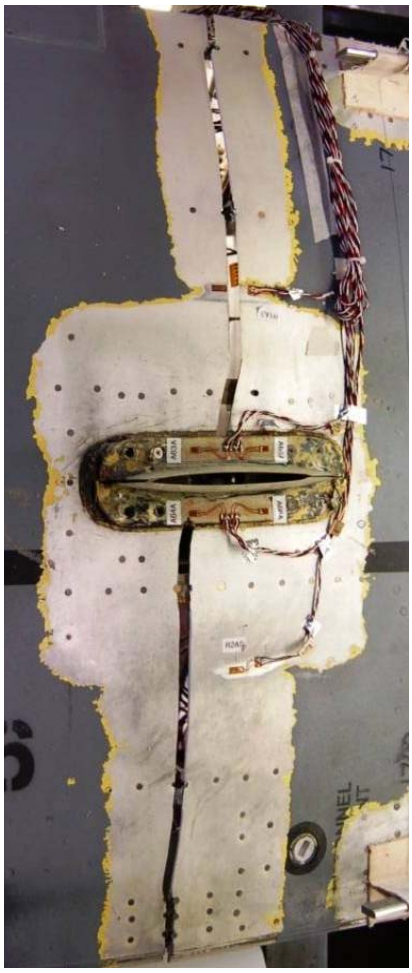

Fig. 21. ST-016 flaw separation after limit load test #2

As with the previous articles, small sections forward and aft of the failure region were cut from the panel and sent to CAStLE for fractographic analysis. All of the stringer faces, as well as the skin outside the flaw region, showed overload failure only.

8.5 Test Articles Overall Test Results Summary

Table 5 shows an overall test results summary of the four test articles.

Table 5. Test articles – overall test results summary

Test Article	Length Size (Frames)	Width Size (Stringers)	Total Fatigue Cycles Applied	Static Residual Strength Applications	Flaw Designation	Flaw Length at Start of Cyclic Testing (in)	Flaw Length Prior to Final Residual Strength Test (in)	Test Article Failure Location
ST-013	6	6	216,500	2	DS1	0.35	0.680	FS 1744 Frame Splice Area
ST-014	6	6	8,770	5	DS2	1.300	5.206	At DS2 Flaw Location
ST-015	6	6	72,180	6	DS1-2	0.501	8.201	At DS1-2 Flaw Location
ST-016	4	6	5,450	2	DS4	4.06*	10.48*	At DS4 Flaw Location

* Visible total overall length of cracks on either side of antenna mast mount.

The residual strength tests showed conclusively that the aft crown structure possesses significantly more crack arrest capability than the legacy residual strength analysis, which were based on finite element and fracture mechanics analyses. These findings confirm that the techniques being employed to manage the operations and maintenance of the C-5 aft crown structure, since they are based on conservative analysis methodologies, provide us with a greater margin of safety than was originally estimated. The critical crack lengths, (at design limit load) demonstrated by test articles ST-014, ST-015 and ST-016 were substantially higher than previous estimates. The test result for ST-013 is considered invalid for measuring the critical crack length because of the extensive damage created away from the test area by the large number of high-stress cycles. However, ST-013 still provided useful data in the form of a known number of stress cycles to develop the multiple site damage. The larger a_{cr} values from the three valid residual strength tests will be accounted for in the Air Force / Lockheed Martin updates to the aft crown risk analyses, and thereby potentially lead to a more economical inspection program.

8.6 NDI Technologies – Conclusions and Assessment Results

The two NDI technologies selected were:

- Semi-automated scanned eddy current
- Ultrasonic array

8.6.1 Semi-Automated Scanned Eddy Current – Test Articles ST-014, ST-015, and ST-016

An initial evaluation concluded that ECSS using semi-automatic scanned eddy current technique and manual scanning were comparable. After reassessment, the semi-automated scanned eddy current system utilized considerably less time, effort, and margin for errors. The three test articles inspected during this examination were completely scanned by the vendor within four days. In contrast, scanning the same test articles utilizing the conventional manual method took more than a week to complete. Additionally, the semi-automated scanned eddy current system revealed other notable advantages as compared to the conventional manual method such as, the assurance of 100% inspection coverage and the availability of real-time C-scan images that can be archived for future referencing.

A few minor issues were noted during the semi-automated scanned eddy current inspection of the test articles. The probe holder used during the inspection was significantly larger in diameter than the actual probe coil.

The large probe holder assisted the probe by maintaining intimate contact with the skin surface and ensured stability during scanning of rough surfaces. In contrast, the diameter of the probe holder precluded the probe from scanning close to large components. This prevented the unit from detecting small cracks propagating from underneath the antenna mast mounts. Quality inspections could not be performed in these areas.

The inspection results from the vendor identified seventeen additional crack indications. Sixteen of the indications were confirmed with ECSS inspection; nevertheless, NIAR will evaluate the area with fluorescent penetrant (FLP) during the post teardown inspection of the test articles. See Table 6 for total count of all confirmed defects.

8.6.2 Ultrasonic Array – Test Articles ST-014, ST-015, and ST-016

An ultrasonic array probe that housed 256 elements in one probe was also used to inspect the test articles. All 256 elements were capable of sending and receiving sound individually. The probe is rather large; however, it allowed rapid inspection of the test articles as compared to a conventional single element probe. The setup process for an initial scan is quite similar to that of a conventional single crystal probe. This allows an experienced ultrasonic (UT) technician to identify and interpret indications without extensive training. In addition, the ultrasonic array is capable of real-time C-scan imaging that can be archived for future referencing.

During the test article examinations using ultrasonic array, there were some noted limitations. As stated earlier, the probe is rather large and flat, which can cause inspection variances on rough and/or curved surfaces. These types of surfaces limited the areas of good contact with the probe which ultimately degraded the inspection quality. Difficulties scanning the slightly curved shape of the test articles were observed during the examination of the first test article.

The inspection results of the three test articles inspected generated fourteen geometry defect indications and twenty-one additional crack indications. No geometry indication was confirmed; only one crack indication (ST-014, Defect 40) was confirmed with ECSS inspection. The geometry indications may have been caused by the substructures which were still attached. Fifteen cracks and two areas of surface corrosion went undetected when comparing the ultrasonic array findings against NIAR in-house results. The largest of the 15 cracks that went undetected measured approximately 0.425 inches long. See Table 6 for total count of all confirmed defects.

Table 6. Total number of confirmed defects using ECSS

Test Article	NIAR	Semi-automated scanned eddy current*	Ultrasonic array*
ST-014	22	20	12
ST-015	16	15	2
ST-016	8	11	3

*Confirmed defects represented defects initially identified by the NIAR in-house process and/or newly identified defects.

8.7 SHM Technologies – Conclusions and Assessment Results

Final selection of SHM technologies was based largely on the overall cost to the program of implementing the systems into the main test program. As a result the following two technologies were incorporated:

- Guided wave ultrasonics
- Acoustic emission

8.7.1 Guided Wave Ultrasonics – Test Article ST-015

The guided wave ultrasonics technology was less mature than was assessed during the selection process. There were a number of issues discovered during the testing that could be resolved in future development but made it difficult to create an objective evaluation.

The sensors lacked a method of maintaining the proper magnetic bias which resulted in variations in signal strength and

prevented interpretation of the resulting signals over time.

Another concern that was identified was the signal response near geometry changes or around complex structure such as the skin splice at FS 1744 on the panels. Between stringers, the sensor signals appeared to channel so that no information could be gained beyond the bay in which the sensor was located. The vendor had predicted this and accounted for it by installing a sensor in each stringer bay. In the complex structure of the skin splice, the sensor signals appeared to echo and did not provide meaningful data for monitoring the structural integrity.

Two of the 128 kHz sensors (sensors 2 and 6) were installed in the stringer bay where the induced flaw was located and provided good data on the flaw location. They also gained signal amplitude as the flaw grew or was mechanically extended. The variations caused by the magnetic bias problem discussed earlier prevented attempts to correlate signal amplitude and flaw size as was desired in the program plan. The data from these two sensors proved there is potential for using this method for large surface areas.

Sensor 3 and sensors 6 through 9 findings include comments on indication locations. These areas were compared to the teardown inspection results. Under sensor 3, an indication was described as "17 inches in the negative direction." The distance indicated was measured from the sensor and negative indicates the direction to be forward on the test article. A crack was found in this area at FS 1699.5. It was an off-axis crack coming out of a fastener and measured 0.130 inches in length. The crack was identified as skin crack 10 on the panel from FS 1675 to FS 1725.25. The indications described under sensors 6 through 9 could not be confirmed as no cracks were found in the areas described.

8.7.2 Acoustic Emission – Test Article ST-014

Significant improvements were made in the test procedure for test article ST-014; which allowed the test to progress rapidly. Unfortunately, this reduced the amount of time that the acoustic emissions system was actually monitoring natural cracking and limited observation of the system and the ability to properly evaluate its operation. Within this narrow scope, the system worked well. A discussion of the observations follows.

The data acquired by the acoustic emission system was filtered and then digitized for initial analysis. When an acoustic emission event was recognized, the data was stored in an event file in ASCII delimited format. A sample of the data from an event is shown in Table 7.

Table 7. Test article ST-014 – sample of acoustic emission data from an event

Channel	Start (sec)	End (sec)	Duration (sec)	Amplitude (volts)	Max Amp Time (sec)
3	11.141584	11.141964	0.000380	2.601	11.141638
2	11.141586	11.141750	0.000164	0.451	11.141633
4	11.141588	11.141862	0.000274	0.904	11.141642
1	11.141626	11.141809	0.000183	0.492	11.141687

Referencing Table 7, the "Channel" column order is the result of when each transducer sensed the event. These data are then further processed to derive location, rate of change, etc. The system software in the acoustic emission unit that was available for test was not compatible with the material being tested, so the automated results were not relative. Manual calculation of the location from the data used triangulation methods, which would normally be in the software, and resulted in properly positioning the induced flaw location.

The acoustic emission system was set up for remote operation, so the only action required by NIAR personnel was to ensure the unit and power supply were turned on. The system was programmed to send NIAR an email so NIAR personnel would know it had passed its self checks and was operating. All other interface with the system was performed by vendor personnel. At one point in the testing vendor personnel noticed a problem in the data from one of the AE sensors. They sent NIAR a note to check the connector on this sensor. The connector had worked loose during the cyclic testing and was repaired by simply retightening the connector. This was impressive that they could accurately remotely recognize and recommend repair of a system problem. They also indicated that on a field installation they have always used hardwired sensors to prevent this issue.

Comparison of the acoustic emission system findings to actual test log and NDI results agreed at each point except one, where both the test log and the acoustic emission system indicated there was crack growth but the timing was different. This was likely a bookkeeping error. Also important to note: there were no false calls during the testing even though the test environment was noisy.

The acoustic emission system appeared to be a good design and, with the exception of additional software development, compatible with metal assemblies and ready for immediate utilization.

9 Contact Author Email Address

The contact author for this paper is:
Melinda Laubach
Director, NIAR Aging Aircraft Lab
Email: Melinda.laubach@wichita.edu

Copyright Statement